Ramsey I. Zeitoun[1]*
Zheng Chen[1]*
Mark A. Burns[1,2]

[1]Department of Chemical Engineering, The University of Michigan, Ann Arbor, MI, USA
[2]Department of Biomedical Engineering, The University of Michigan, Ann Arbor, MI, USA

Received March 28, 2008
Revised July 7, 2008
Accepted July 11, 2008

Research Article

Transverse imaging and simulation of dsDNA electrophoresis in microfabricated glass channels

We have observed the non-uniform distribution of DNA molecules during PAGE in a microfabricated system. Confocal laser scanning microscopy was used to visualize fluorescently labeled DNA during electrophoretic migration. The distribution of double-stranded DNA larger than 100 bp is observed to transition from a center-biased motion on the transverse plane 1 cm downstream from injection to an edge-biased motion 2 cm downstream. Although this distribution increased with increasing dsDNA size in a cross-linked gel, no similar distribution was found with the same dsDNA molecules in a linear polyacrylamide solution (6%). Simulations of DNA distribution in gels suggest that DNA distribution non-uniformities may be caused by biased electrophoretic migration resulting from motion in an inhomogeneous gel system.

Keywords:
Biased reptation model / Confocal laser scanning microscope / DNA electrophoresis / Transverse detection
DOI 10.1002/elps.200800204

1 Introduction

Polyacrylamide electrophoresis of DNA is used in a wide range of applications including genetic analysis, mutation detection, disease diagnosis, and forensic screening. This separation technique has been adapted by the emerging lab-on-a-chip systems in recent years and serves as the principal separation component of many microfluidic-based bioanalysis systems [1–5]. Cross-linked polyacrylamide is particularly attractive mainly due to its relatively short required separation distances as compared with other matrices [6, 7]. The resolution of these systems has been optimized by several means, including electrode-compaction injection [8], on-chip fabricated detectors [9], and the introduction of buffer flow [10]. The resolving power has been improved to a comparable level as that achieved by linear polymer solutions but at distances considerably shorter [11].

However, there are other problems associated with cross-linked polyacrylamide. For instance, we have previously observed a loss in resolution for dsDNA bands larger than 200 bp in relatively dense gels (10%T) [10] or dsDNA bands larger than 500 bp in less-concentrated gels (5%T) [6]. This reduction significantly limits the resolvable size range of dsDNA especially in microfabricated devices with pre-loaded gels. Also, the microstructure of some cross-linked gels was found to be inhomogeneous [12], a phenomena that could be dependent on the monomer and cross-linker's concentrations as well as the polymerization process [13].

Continuous 3-D visualization of electrophoretic motion in gels can aid in understanding these and other aberrant migration patterns. de Carmejane *et al.* have studied long-chain DNA (T2, 164 kbp) interacting with surrounding polymer fibers (0.38% HEC, 1 × TBE) in a 3-D manner by taking spatially separated cross-sectional fluorescence images and reconstructing them into a 3-D image [14]. Advancements in microscope technology make continuous 3-D visualization (*xyzt*) possible. Confocal laser scanning microscopy, which has been widely used in the field of molecular biology, cell biology, and colloidal particle research, was also used for the detection of ssDNA electrophoresis in a slab-gel [15] and in a microfabricated disc [16]. However, these studies were limited to the observation of ssDNA on the conventional detection plane (*x*–*y*). To our knowledge, dsDNA gel electrophoresis in cross-linked gels has never been observed on a transverse plane.

We observed dsDNA motion during electrophoresis in microfabricated glass channels using confocal laser scanning microscopy. Both cross-linked and linear polyacrylamide (LPA) matrices were used as well as various lengths of dsDNA. To support and better understand our findings we also developed a reptation simulation model that predicts DNA's position in small-pore gel environments during electrophoresis.

Correspondence: Professor Mark A. Burns, Department of Chemical Engineering, The University of Michigan, Ann Arbor, MI 48109, USA
E-mail: maburns@umich.edu
Fax: +1-734-763-0459

Abbreviation: LPA, linear polyacrylamide

*These authors contributed equally to this work.

2 Materials and methods

2.1 Microchannel etching

Two designs of microchannel geometries were used in experiments, as shown in Fig. 1A. Design A was only used for dsDNA electrophoresis using LPA solution. Design B (Fig. 1B) was used for electrophoresis of all other samples. Microchannels were etched on 500 μm thick, 4 in. borofloat glass wafers (Precision Glass and Optics, Santa Ana, CA, USA). First, wafers were pre-annealed in a furnace by slowly ramping the temperature to 600°C and holding it overnight. After annealing, 500 Å of chromium followed by 3500 Å of gold were deposited on the float surface of each glass wafer. The wafers were then spin-coated with Microposit SC1827 positive photoresist (Shipley, Marlborough, MA, USA), patterned with the desired channel design and developed in MF319 photoresist developer (Shipley).

Metal layers were etched with gold etchant TFA (Transene, Danvers, MA, USA) followed by CR-14 chromium etchant (Cyantek, Fremont, CA, USA). Glass features were then etched by immersing the patterned wafer into 49% hydrofluoric acid solution for 5–15 min to give a series of channel depths (with channel width equal to 50 μm plus two times the channel depth). The channel depth was measured by a stylus surface profilometer and was around 50 μm for a 10 min etch.

2.2 Device assembly

After the channels were etched, holes were drilled through the reservoirs on the glass side by electrochemical spark discharge. For devices assembled with glass-to-glass thermal bonding, 500-μm thick glass wafers with etched features and 100-μm thick Pyrex 7740 glass wafers (Sensor Prep Services, Elburn, IL, USA) were cleaned in 3:1 sulfuric acid/hydrogen peroxide solution for 25 min. Following, both pieces were soaked in potassium hydroxide solution (40% electronic purity) at 85°C for 15 min then liberally rinsed with deionized water. Then, the wafers were gently dried with nitrogen, pressed together by two Macor ceramic plates (Ceramic Products, Palisades Park, NJ, USA) and thermally bonded in an oven for 5 h at 560°C.

Thermally bonded wafers were diced into individual pieces for use. Buffer reservoirs and fittings for external electrodes were attached with SK-9 Lens Bond UV curable optical glue (Summers Optics, Fort Washington, PA, USA). For devices assembled by UV-glue, glass wafers with etched features were first diced, then bonded to another piece of Pyrex 7740 with SK-9, and finally cured under UV-light. UV-cured devices were occasionally reused. To accomplish this, the etched glass side was separated from the bonded wafer and channels were cleaned by razorblade agitation along with water, ethanol, and isopropanol.

2.3 Channel treatment

Devices assembled by glass-to-glass thermal bonding were used without further cleaning. All devices assembled by UV-glue were rinsed with water followed by ethanol and dried by vacuum aspirator. All channels were pretreated following the protocol developed by Hjerten [17]. After channel treatment, the device was dried in a desiccator before use.

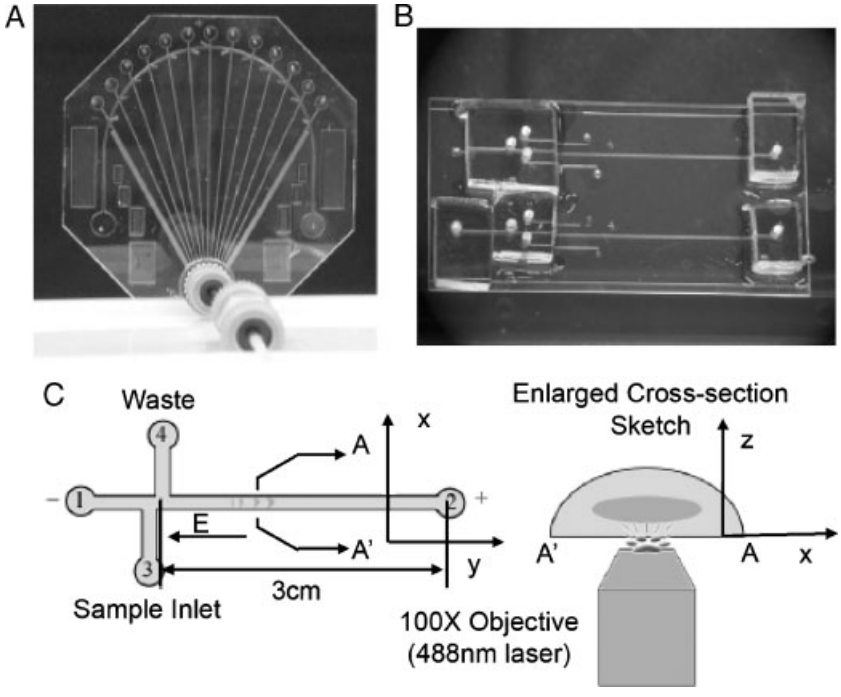

Figure 1. The photo images of the microfabricated devices used in the study of DNA electrophoresis with confocal laser scanning microscope: (A) Design I; (B) Design II; (C) sketch of confocal microscopy scanning mode and cross-section of microchannel with definition of coordinates: *x*-; *y*-length of the channel, *z*-depth of the channel.

2.4 Gel preparation

Polyacrylamide (8%T) was made from a mixture of ReprolGel^{TM} High Resolution Solutions A and B (Amersham Pharmacia Biotech, Piscataway, NJ, USA) according to the manufacturer's instruction. Polyacrylamide gel of varying monomer/cross-linker concentrations was formed by diluting ReprolGel^{TM} High Resolution formula with 1 × TBE buffer solution. For thermal studies, polyacrylamide with pre-mixed Rhodamine B was made by mixing 190 μL 8% ReprolGel^{TM} Solutions A and B with 10 μL 0.4 mM Rhodamine B (in 10 × TBE buffer) to a composition of 7.6%T and 0.02 mM Rhodamine B.

Prior to UV-polymerization, freshly mixed monomer and initiator solution was degassed in a desiccator for 30 min. The solution was then loaded into the microchannel by pipette. A distinct gel interface was created following work previously published by Brahmasandra *et al.* [8]. A model XL-1000 spectrolinker UV cross-linker (Spectronic, Westbury, NY, USA) was used for UV-initiation and gel polymerization. The solution was first exposed to UV-light source for a 100 s pre-polymerization. Then, 10 μL 1 × TBE buffer was added into the buffer tanks at both ends of the separation channel (Fig. 1) to balance the ionic concentration and keep the gel interface moisturized during gel formation. For complete polymerization, an additional 600 s of UV exposure was applied. After gel polymerization, the chip was set with both ends filled with 30 μL fresh 1 × TBE solution for at least 30 min until use.

LPA solution, 6%T, was degassed by helium flow for 5 min and loaded into the microchannel by high pressure helium through tubing connections and NanoPort^{TM} fittings (Upchurch Scientific, Oak Harbor, WA, USA), as shown in Fig. 1A.

2.5 Sample preparation

The 20 and 100 bp dsDNA size-standards were commercially purchased (Bio-Rad, St. Louis, MO, USA). Monodispersed dsDNA samples (343 and 462 bp) were amplified from mouse RNA by PCR and diluted with deionized water at a 1:5 ratio of DNA to water. dsDNA samples were labeled with YOYO-1 intercalating dye (Molecular Probes, Eugene, OR, USA) at a volume ratio of 2:1 ratio of dye to DNA. All light-sensitive samples were kept in the dark after preparation.

2.6 LabVIEW^{TM} controlled injection and electrophoresis

The electrophoresis apparatus included a computer loaded with LabVIEW^{TM} software, data acquisition card, stage adaptor for mounting the chip on the confocal microscope stage, circuit connections and controls, a BHK-2000-20MG high-voltage power supply (Kepco, Flushing, NY, USA) and microfabricated devices. A LabVIEW^{TM} program was used for control of a three-phase, electrokinetic injection and electrophoresis process. A diagram of the system is displayed in Fig. 1C. Prior to electrokinetic injection, a 0.5 μL sample, labeled with fluorescent dye, was loaded into port 3. To begin, a +20 V potential was applied on port 4 for 2 s while ports 1, 2 and 3 were grounded to move the sample into the channel intersection area. Next, a +150 V potential was applied on port 2 for 0.5 s with port 1 grounded, to move the sample plug into the separation channel. Meanwhile, a +10 V anti-leakage potential was applied on port 4. Finally, the +150 V potential was kept on port 2 for sample electrophoresis toward port 2, while a +20 V potential was applied on ports 3 and 4 to hold all uninjected sample at the intersection area and prevent tailing while port 1 was kept grounded.

2.7 Detection with confocal microscopy

DNA and fluorescein-Na electrophoresis were monitored by a Leica SP2 confocal laser scanning microscope (Leica Microsystems, USA) with a 100 × /1.40–0.70 objective. The green fluorescent signal (YOYO-1) was excited with an Ar/ArKr laser (488 nm) while the red signal (Rhodamine B) was excited with a He/Ne laser (543 nm). A single- or dual-channel transmission detector was used according to the detection needs.

xzt-scanning mode was used to scan the channel cross-section. The scanning speed was set at 400 MHz (~1.68 s/frame), giving an image resolution of 512 × 512 pixels. Image gain and offset were adjusted to a proper level and kept constant for the rest of the detection. The motorized x–y stage was controlled either by a joystick, for fast movement, or knob, for fine movement. Movement along the z-axis for scanning used the galvanometric z-stage controlled *via* software.

2.8 Image process and data analysis

All the images were taken and digitalized by Leica confocal software (Leica Microsystems). Image processing and profile plots were constructed with Photoshop v9.0 (Adobe, USA) and MATLAB (MathWorks, Inc. Natick, MA, USA). Using Photoshop and MATLAB, the intensity profile of the cross-section was plotted by selecting a measuring window, which is a rectangular section covering the center area of the cross-section from the bottom to top of the channel. Subsequent distribution calculations of the extracted image were completed with MATLAB.

2.9 Simulation of dsDNA movement

dsDNA's transverse movement was simulated using MATLAB software on a Pentium 4 desktop (Dell, USA).

Random number generation was obtained from MATLAB's 'rand' command. An electric field of 5 kV/m was used, corresponding to a 150 V potential across a 3 cm gap. The linear charge density used is 2 eV/bp of DNA. The ambient temperature was set to 298 K, and the Kuhn length of dsDNA used was 100 nm.

3 Results and discussion

3.1 Observation of non-uniform DNA distribution

During electrophoresis, dsDNA is distributed non-uniformly in photopolymerized cross-linked polyacrylamide gels. We observed that as dsDNA migrates from cathode to anode it is initially concentrated in the center and then gradually separates to the top and bottom of the gel. Figure 2 shows the cross-sectional migration of a 343 bp dsDNA band that displays this center-concentrated (1 cm from injection) to edge-concentrated (2 cm) transition. Similar distribution patterns were observed for both 343 and 462 bp dsDNA bands. This phenomenon is a strong function of DNA's migration distance. When observing the migration of a 20 bp ladder for over 30 min, the center-concentrated and edge-concentrated distributions did not change as a function

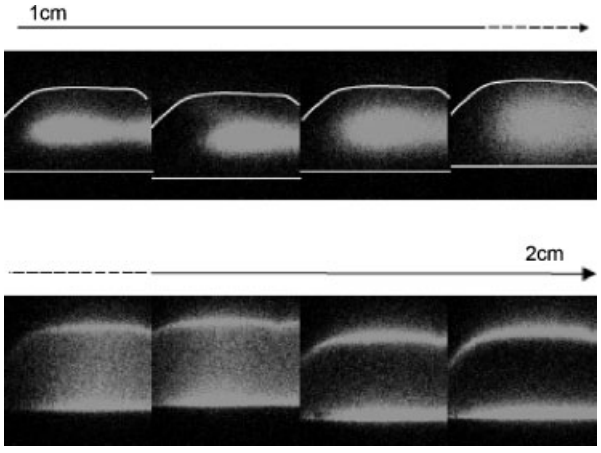

Figure 2. DNA distribution (343 bp, 8%T polyacrylamide gel) in the cross-sectional plane of the microchannel, and its net transverse movement as a function of *y*-distance (detected by moving the stage along DNA migration direction in ~2 min).

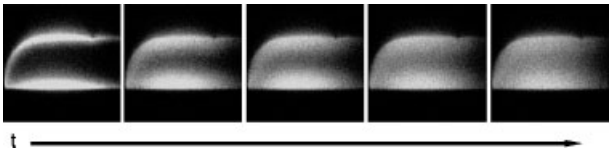

Figure 3. Images of self-diffusion (8% polyacrylamide gel) induced distribution change when the electric field turned off viewed at 2 cm from injection. The first image is taken right after the turn-off of the electric field (*e.g.* $t_d = 0$ min) and each image is taken 1 min after the previous one (*e.g.* the last image represents the distribution at the moment $t_d = 4$ min).

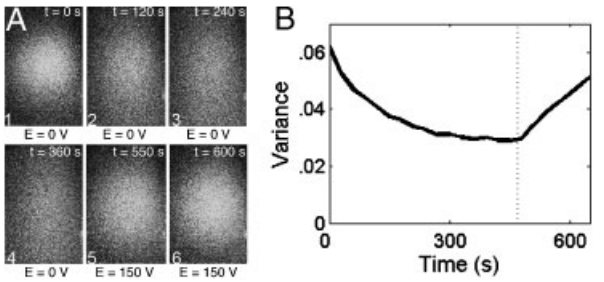

Figure 4. (A) Center-concentrated DNA pattern (1 cm from injection, 8% polyacrylamide gel) as a 150 V electric field is cycled. At image 1 ($t = 0$) the electric field is shut off, subsequent images are displayed 120 s apart. Image 6 ($t = 600$ s) after the field is reapplied, the center-concentrated pattern returned to near full strength. Image times are approximate. (B) Variance of the images *versus* time. Fluorescence intensity was integrated across the width of the channel, then variance was calculated from integrated width intensity with respect to the height of the channel. The dotted line represents reapplication of the electric field.

of migration time. In addition, DNA distribution occurs primarily on the top and bottom of the gel rather than the sides, suggesting that the distribution could be caused by a channel geometric effect or a gel polymerization side effect.

The non-uniform distribution is an active process and not a passive distribution. The edge-concentrated DNA distribution pattern of a 343 bp migrating band was monitored as the applied electric field was terminated. As seen in Fig. 3, dsDNA immediately begins to diffuse into areas of lower concentration. In the absence of an electric field, distributed DNA patterns disperse in approximately 5 min. Once the field is reactivated, the DNA distribution pattern returned to its initial distribution state in both the center-concentrated (Fig. 4A) and edge-concentrated perspectives. Note that the decay of the distribution, measured by each image's variance of fluorescence intensity with respect to the vertical direction (Fig. 4B), shows a first-order decay. This functionality is different when the field is reapplied; the variance linearly increases with time.

3.2 Factors influencing DNA distribution

Interactions between migrating DNA and its surrounding gel matrix influence the distribution. We investigated several factors that might affect the migration of DNA including the DNA length, the cross-linking properties of the gel, the monomer density, and the presence of any temperature gradients. For example, different dsDNA distribution intensities were observed using individual lengths of DNA ranging from 20 to 462 bp in addition to a 20 bp ladder. As seen in Fig. 5A–D, 20 bp dsDNA strands whose lengths are on the order of the gel pore size migrate uniformly. However, as dsDNA length increases, DNA begins to migrate in a biased fashion. dsDNA, sized from 100 to 462 bp, display both a center-concentrated and

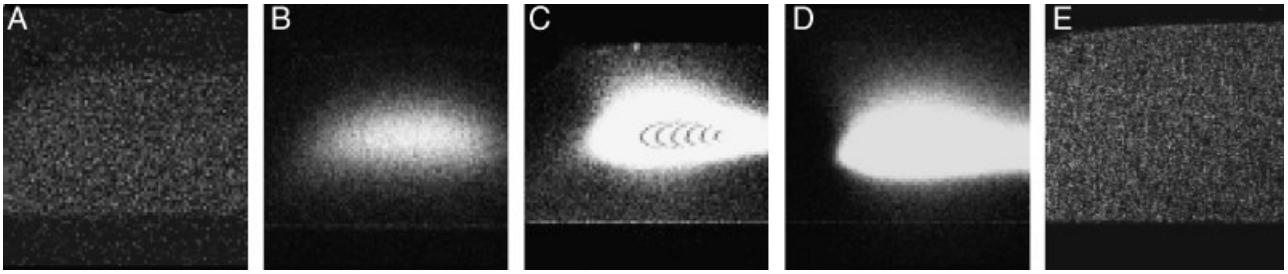

Figure 5. Various distribution patterns of dsDNA on the cross-sectional plane corresponding to the size of DNA strands and gel type. (A) 8%T 20 bp; (B) 8%T 100 bp; (C) 8%T 343 bp; (D) 8%T 462 bp; (E) 6% linear polyacrylamide 200 bp. (A)–(D) are taken 1 cm downstream of starting point of the electrophoresis while (E) was chosen as a representative image.

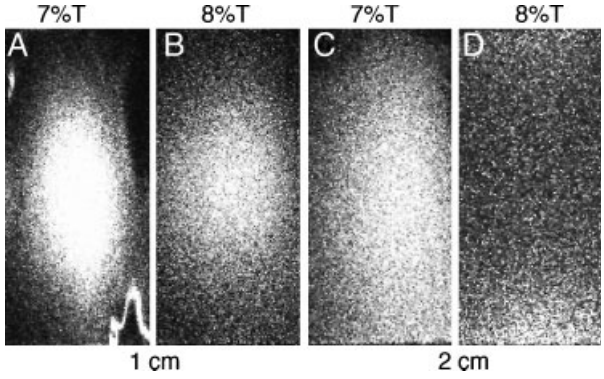

Figure 6. Distribution images of a 20 bp DNA ladder migrating through both 7%T and 8%T polyacrylamide gel at $t \sim 30$ min: (A) 7%T 1 cm after injection; (B) 8%T 1 cm after injection; (C) 7%T 2 cm after injection; (D) 8%T 2 cm after injection.

edge-concentrated distribution bias as a function of migration distance. Hundred base pair dsDNA was less intensely concentrated along the gel edges than 343 and 462 bp strands. Note that in a more elastic network, such as 6% LPA solution (Fig. 5E), we observed no concentration gradients.

The distribution of DNA was also a function of pore size. To vary pore sizes, gels with concentrations 7%T (larger pores) and 8%T (smaller pores) were used. Gel structures have been investigated by various groups and have been shown to have a bulk pore size, for these concentrations, ranging between 5 and 10 nm [18]. As displayed in Fig. 6, 7%T (Fig. 6A) and 8%T (Fig. 6B) gels were observed to be center-concentrated at 1 cm. However, the transition from center-concentration to edge-concentration does not occur at the same distance for both systems. Two centimeters after injection, in 7%T gel (Fig. 6C), DNA is in a transition state similar to intermediate pictures seen in Fig. 2, *versus* 1.5 cm for the 8%T gel.

Non-uniform DNA distribution does not appear to be a result of electroosmotic flow or thermal gradients caused by Joule heating. dsDNA migration patterns were studied in both a bare glass channel and in a channel with covalently coated acrylamide monomer as described in Section 2 and Ref. [17]. Within 2 cm of observed migrations, the distributions of a 343 bp dsDNA band were unchanged in both cases. Thermal gradients were measured using Rhodamine B, a thermo-fluorescent dye. Initial fluorescence signals were compared with those taken 30 min after the 150 V electric current was applied. There was only a slight decrease (8%) in the overall intensity, corresponding to less than 5°C increase in the gel temperature according to the slope reported by Ross *et al.* [19].

3.3 Simulation of DNA's transverse movement

A simulation was developed that employs principles of the biased reptation model to aid in understanding the observed dsDNA distribution. The simulation models dsDNA as a strand made up of several interconnected segments [20]. Because dsDNA reptating through cross-linked polyacrylamide gel (pores ~5–90 nm) has a Kuhn length (~100 nm) larger than the gel matrix's pores, the motion is modeled as a rigid fluctuating head segment leading a number of other segments as they migrate through a gel [21–25].

A Boltzmann distribution based on bending and electrostatic forces determines the probability of specific alignments of the dsDNA's head segment:

$$p_i = \frac{\exp(\sigma \cdot \Delta\hat{n}_i^2)}{\sum_j^N \exp(\sigma \cdot \Delta\hat{n}_j^2)} \cdot \frac{\exp(-\epsilon/2(1-\hat{n}_{x,i}))}{\sum_k^N \exp(-\epsilon/2(1-\hat{n}_{x,k}))}; \quad \sigma = \frac{b}{a}; \quad \epsilon = \frac{qEa}{k_b T} \tag{1}$$

where $p(E, q, a, b, T, n)$ is a function of the electric field, segment charge, pore size, persistence length, temperature, and current alignment [23, 26–27]. This probability results from a strand's change in energy from both disengagements with the electric field and bends between stiff interconnected segments *versus* thermal fluctuations. For each step, a new orientation angle and direction of movement is selected based on MATLAB random number generation *versus* the probability of selecting a corresponding alignment. Once an angle is selected, DNA is moved one segment length and the head alignment is re-evaluated. At walls, DNA can sample fewer angles because of steric interactions, so the probability of choosing an impossible alignment is automatically set to zero. After a new align-

ment is chosen, the strand is moved in the direction of that alignment for one pore distance. This process is repeated for multiple DNA strands and time-steps.

Simulations show DNA's movement changes significantly between gel systems (50 μm channels) with different pore sizes (Fig. 7). For small pores (5 nm, $\varepsilon = 0.0022$, $\sigma = 16$), the dsDNA's resistance to bending governs and results in slower, variable motion. For larger pores (80 nm, $\varepsilon = 0.5632$, $\sigma = 1.25$), the electrostatic forces dominate and the molecules align more with the field, resulting in quicker, more uniform movement. Trajectories of individual DNA molecules (data not shown) show that DNA exhibits more transverse movement in small pores than in large pores. This can also be seen in Fig. 7, where the larger band dispersion in a small pore system is indicative of more transverse motion.

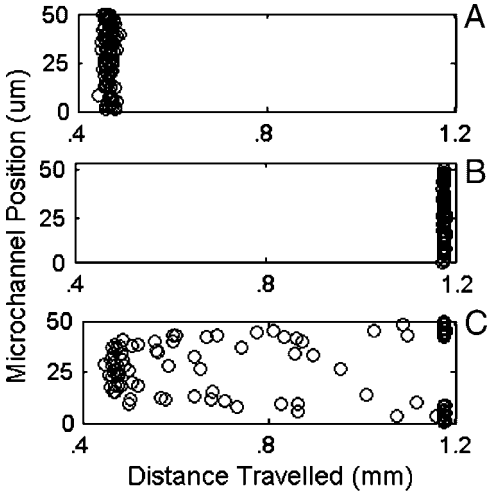

Figure 7. Images of 100 strands of DNA (350 bp) after $t = 5$ s in (A) 5 nm pores, (B) 80 nm pores, (C) 80 nm pores (10 μm on the top and bottom of the channel) and 5 nm pores (occupying the center 30 μm).

We simulated a binary-pore system and found that this produced both center-distributed and edge-distributed DNA patterns, similar to what has been observed. A binary-pore system was chosen because TEM imaging has shown that cross-linked polyacrylamide gel polymerized in enclosed glass channels form larger pores near the walls and smaller pores near the center [12]. In multipore systems, distribution results from DNA in small pores being more likely to migrate transverse to the electric field *versus* large pores that are more likely to align with the electric field. The results (Fig. 7C) demonstrate that DNA on the edges travel faster and may be observed before the center DNA reaches a fixed detection point. As DNA migrates (Fig. 8A), DNA in the smaller, center pores begins to move to the edges, creating a 3-D, parabolic concentration gradient similar to what is observed in Fig. 2. Also, the DNA distributes non-uniformly across the gel; the number of DNA molecules in the center decreases while the number of DNA molecules at the edges increase (Fig. 8B). In addition to representing the confocal data, these simulated data also resemble separations performed earlier by Brahmasandra *et al.*, where they acknowledged the 2-D parabolic shape to unpolymerized gel at the channel edges [8].

4 Concluding remarks

In this paper, we report on our observation of transverse DNA electrophoretic migration in cross-linked polyacrylamide gel polymerized in microfabricated glass channels. With the primary gels we studied (8%T and 7%T *in situ* UV-initiated cross-linked polyacrylamide), a center-biased pattern is observed for detection at a relatively short migration distance (1 cm) while an edge biased is observed at a longer migration distances (2 cm) for dsDNA. The distribution becomes weak or even disappears as the size of dsDNA decreases to the scale of the pore size or if an LPA solution is used.

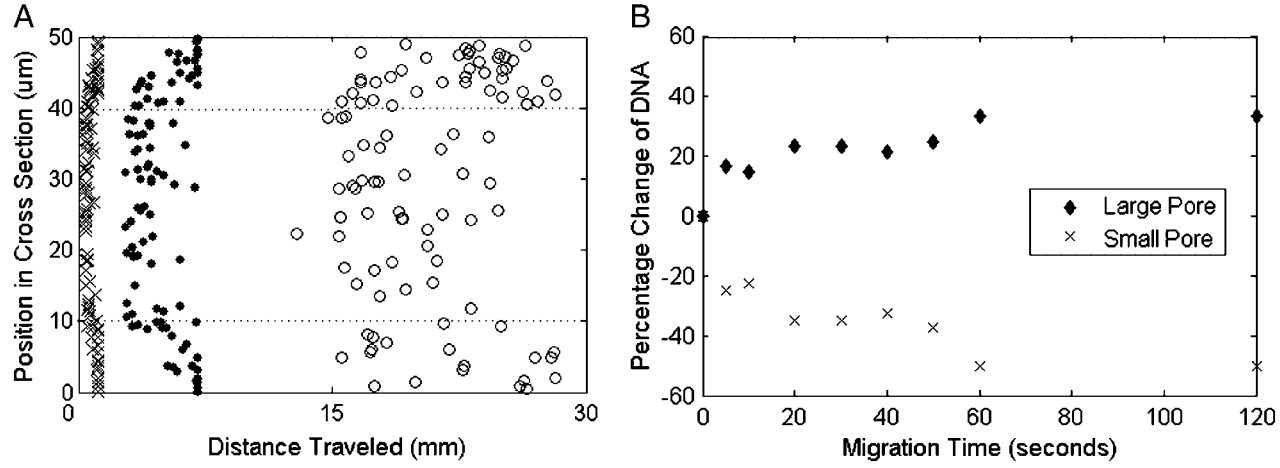

Figure 8. (A) DNA traveling through a stratified pore system over different time-lapses (×) 5 s; (●) 30 s; (O) 120 s. Dotted lines represent the large and small pore interfaces. (B) Percentage change $100 \times (N - N_o)$/No. of DNA in large pores (◆) and small pores (×) *versus* time.

Our simulations show that a multipore gel with large pores near the walls and smaller pores in the interior will produce an edge-concentrated and center-concentrated DNA pattern. This preliminary result is also consistent with the observation that as the pore size increases (*i.e.*, monomer concentration decreases), the transition from center-concentration to edge-concentration becomes more gradual. In addition, the observed DNA distribution is an active process (Fig. 4B) and an inhomogeneous gel may be a contributing factor. Although the experimental and simulated results coincide fairly well, neither accounts for the reversibility of DNA distribution nor the absence of the edge distribution at shorter (1 cm) distances. The possibility of an entropic trapping mechanism may help account for these observations and would be interesting to study in the future.

By understanding the mechanism that causes distribution we can design channels and gels that favor more uniform migration. For instance, designing systems to mitigate pore size inhomogeneities, such as changing channel aspect ratios and the polymerization procedure can be taken into account in future designs and expand the versatility of microfabricated separation systems. However, many additional experiments and simulations need to be performed before the exact causes of the observed DNA distributions can be stated with confidence. High-resolution imaging of the gel pore structure would help corroborate or negate the pore size arguments and other parameters such as electric field gradient and nonhomogeneous field gradients in the channels could be explored. Although additional work is necessary to fully understand migration behavior in these gels, the high resolution separation in extremely short distances that are possible with cross-linked polyacrylamide gel continue to reinforce cross-linked polyacrylamide gel as a useful separation medium and strong compliment to other media such as LPA solution.

We gratefully acknowledge Brian N. Johnson, for the assistance on LabVIEW™ control. We also would like to thank Sean Langelier and Dustin Chang for many thoughtful discussions on the topics. Additional thanks to Thomas Westerich and Eric Shpritz for comprehensive readings of the paper. The work is supported by the National Human Genome Research Institutes (Grant P01 HG01984) and Infectious Diseases (Grant R01 AI49541) of the National Institutes of Health.

The authors have declared no conflict of interest.

5 References

[1] Waters, L. C., Jacobson, S. C., Kroutchinina, N., Khandurina, J. *et al.*, *Anal. Chem.* 1998, *70*, 5172–5176.

[2] Khandurina, J., McKnight, T. E., Jacobson, S. C., Waters, L. C. *et al.*, *Anal. Chem.* 2000, *72*, 2995–3000.

[3] Lagally, E. T., Scherer, J. R., Blazej, R. G., Toriello, N. M. *et al.*, *Anal. Chem.* 2004, *76*, 3162–3170.

[4] Kan, C. W., Fredlake, C. P., Doherty, E. A., Barron, A. E., *Electrophoresis* 2004, *25*, 3564–3588.

[5] Pal, R., Yang, M., Lin, R., Johnson, B. N. *et al.*, *Lab Chip* 2005, *5*, 1024–1032.

[6] Ugaz, V. M., Lin, R., Srivastava, N., Burke, D. T. *et al.*, *Electrophoresis* 2003, *24*, 151–157.

[7] Koutny, L., Schmalzing, D., Salas-Solano, O., El-Difrawy, S. *et al.*, *Anal. Chem.* 2000, *72*, 3388–3391.

[8] Brahmasandra, S. N., Ugaz, V. M., Burke, D. T., Mastroangelo, C. H. *et al.*, *Electrophoresis* 2001, *22*, 300–311.

[9] Namasivayam, V., Lin, R. S., Johnson, B., Brahmasandra, S. *et al.*, *J. Micromech. Microeng.* 2004, *14*, 81–90.

[10] Chen, Z., Burns, M. A., *Electrophoresis* 2005, *26*, 4718–4728.

[11] Salas-Solano, O., Schmalzing, D., Koutny, L., Buonocore, S. *et al.*, *Anal. Chem.* 2000, *72*, 3129–3137.

[12] Ruchel, R., Steere, R. L., Erbe, E. F., *J. Chromatogr.* 1978, *166*, 563–575.

[13] Ikkai, F., Shibayama, M. J., *Polym. Sci. B: Polym. Phys.* 2005, *43*, 617–628.

[14] de Carmejane, O., Yamaguchi, Y., Todorov, T. I., Morris, M. D., *Electrophoresis* 2001, *22*, 2433–2441.

[15] Djouadi, Z., Bottani, S., Duval, M. A., Siebert, R. *et al.*, *Electrophoresis* 2001, *22*, 3527–3532.

[16] Emrich, C. A., Tian, H., Medintz, I. L., Mathies, R. A., *Anal. Chem.* 2002, *74*, 5076–5083.

[17] Hjerten, S., *J. Chromatogr.* 1985, *347*, 191–198.

[18] Chen, Z., Improving electrophoretic resolution in microfabricated bioanalysis devices. PhD thesis, University of Michigan, Ann Arbor 2007.

[19] Ross, D., Gaitan, M., Locascio, L. E., *Anal. Chem.* 2001, *73*, 4117–4123.

[20] Lumpkin, O. J., Dejardin, P., Zimm, Z. H., *Biopolymers* 1985, *24*, 1573–1593.

[21] Viovy, J. L., *Rev. Mod. Phys.* 2000, *72*, 813–866.

[22] Lumpkin, O. J., Zimm, B. H., *Biopolymers* 1982, *21*, 2315–2316.

[23] Semenov, A. N., Duke, T. A., Viovy, J. L., *Phys. Rev. E* 1995, *51*, 1520–1537.

[24] Duke, T. A., Semenov, A. N., Viovy, J. L., *Phys. Rev. Lett.* 1992, *69*, 3260–3263.

[25] Semenov, A. N., Subbotin, A. V., *Polym. Sci. USSR* 1990, *32*, 1208–1214.

[26] Semenov, A. N., Subbotin, A. V., *Polym. Sci. USSR* 1989, *31*, 2811–2818.

[27] Subbotin, A. V., Semenov, A. N., *Electrophoresis* 1996, *17*, 1018–1026.

